New Observables of the Cosmic Microwave Background

Marco Lanucara (marco.lanucara@esa.int)
European Space Agency
Robert Daddato
European Space Agency

Research Article

Keywords:

Posted Date: May 3rd, 2022

DOI: https://doi.org/10.21203/rs.3.rs-1585609/v1

New Observables of the Cosmic Microwave Background

Marco Lanucara and Robert J. Daddato

Authors information
Affiliations
European Space Agency, Robert-Bosch-Str. 5, D-64293 Darmstadt, Germany
Marco Lanucara, email to marco.lanucara@esa.int
Robert J. Daddato, email to robert.daddato@esa.int

Corresponding author: Marco Lanucara

Abstract

We introduce new observables of the cosmic microwave background radiation, which can be measured through the detection of high order modes excited within an antenna feed system, coherently combined with those currently detected by space observatories. The use of such observables could potentially further constrain the validity of cosmological theories.

1. Introduction

Experiments in the past have aimed at measuring the temperature of the cosmic microwave background (CMB) radiation, after its experimental discovery by Penzias and Wilson in 1965 [1]. A historical review of such experiments is provided in [2]. When limiting our attention to space observatories, we can recall the RELIKT-1 mission [3] operating during 1983-1984, the Cosmic Background Explorer [4] (COBE, 1989 to 1993), the Wilkinson Microwave Anisotropy Probe [5] (WMAP, 2001 to 2010) and the Plank mission [6] (2009 – 2015).

In all such experiments the temperature of the CMB was measured over an angular grid across the celestial sphere, with ever increasing level of accuracy, angular resolution and angular coverage. When grouping the many specificities of each mission (calibration methods, angular and spectral coverage etc.), into one long-term effort, it can be stated that a common principle was followed, to measure the power of the radiation observed by an antenna system, and to relate such measurement to the structure of the temperature field in the angular surrounding of the antenna boresight. Multiple feeds and associated detection mechanisms could ensure the coverage of several frequency bands as well as orthogonal polarisations, and the measurement was conducted over a grid of angular directions, allowing the reconstruction of the whole temperature field.

The goal of the present paper is to complement the above measurement with additional observables which can also be related to the structure of the temperature field. The approach is to detect high order modes in the feed system, which are excited, together with the dominant mode (the one used already), by the impinging radiation and that typically do not propagate beyond the feed system. Such modes carry information about the radiation, they can be extracted and coherently combined with the dominant mode to form useful observables. Such high order modes are already used in other fields, e.g., for tracking systems used to identify and track the direction of arrival of radio emitters, and the present paper shows how their use can be extended to the characterisation of the CMB.

The paper is organised as follows: In section 2 the methodology which has been used for past missions is discussed, with a focus on the main principles and ideas. The objective is to recall few key assumptions which are necessary when interpreting the measured observable, and which are also required for using the newly proposed ones. In section 3 the new observables are introduced. Section 4 describes the approach for a sample antenna system, limiting the discussion to two high order modes. Concluding remarks and hints for future work are reported in section 5.

2. Considerations about the current CMB observable

Past space observatories have characterised the CMB by measuring the power received by an antenna system over a grid of angular directions, with a time integration required to suppress the measurement noise. In order to discuss the methodology, let us focus on one individual measurement conducted over a fixed orientation, and define a reference frame solidly with the antenna system as depicted in fig. 1, with angular coordinates θ, ϕ such that for example the zero of the polar angle θ corresponds to the antenna boresight. Similarly, the CMB temperature field (and in particular its fluctuation ΔT around a mean) can be expressed as a function of the two above angular coordinates θ and ϕ, possibly after a coordinate transformation from a standard (e.g., cosmological) reference frame

$$T(\theta, \phi) = \bar{T} + \Delta T(\theta, \phi). \tag{1}$$

In the above definition $\bar{T}$ is the mean value, measured to be $2.72548 \pm 0.00057\ K$[7], and ΔT is the fluctuation about the mean. We assume that the antenna feed system has two output ports, reacting to orthogonal polarisation states of the incoming radiation. When random unpolarised radiation is observed, the power is split equally across the two ports, however this is not necessarily the case and it depends upon the physical properties of the source. In the following we will not address polarisation issues in particular, with the understanding that any related consideration applicable to the current methodology can be extended to the new one.

The measurement of the CMB temperature is performed through the conceptual setup depicted in fig. 1, consisting of a low noise power amplifier connected to a feed output port, followed by filtering, frequency down conversion to complex baseband and power measurement (all above duplicated to account for two orthogonal polarisations). The described setup is an idealisation, and may differ from other methods, *e.g.* the connection of bolometers to each feed output port for direct power measurement [8], without need of frequency down-conversion. Furthermore, use of calibration loads is required, to take into consideration 1/f noise from the electronics [9]. However, provided that one is considering an idealised system, the various methods of measuring the signal power within a pre-selected bandwidth are equivalent, and the merit of the one illustrated in fig. 1 is to allow an extension to the use of high order modes, which is the actual subject of this paper, and is discussed in the next section.

The signal available at the power measurement point shown in fig. 1 is made up of a contribution due to the internal noise from the feed and electronics, and the contribution due to the CMB temperature. We assume for the moment that the CMB temperature is different from zero only at a point source along the direction θ, ϕ within a small solid angle $\delta\Omega$, within the antenna reference frame. In such scenario the received power is expressed as follows

$$[\text{received power}]_{\text{point source}} = g_x W k \left(\frac{1}{4\pi} T(\theta, \phi) G(\theta, \phi) \delta\Omega + T_R \right), \tag{2}$$

where k is the Boltzmann constant, W is the bandwidth within which the power is measured. The black-body spectral radiance is assumed to follow the Rayleigh–Jeans approximation. The term $G(\theta, \phi)$ represents the value of the antenna gain in the direction θ, ϕ, essentially the antenna far-field radiation pattern in its own reference frame, and finally the noise temperature T_R represents the noise introduced by the lossy feed and by the full electronics chain, within the measurement bandwidth. The term g_x denotes the power gain of the electronics, from the input of the low noise amplifier down to the power measurement point.

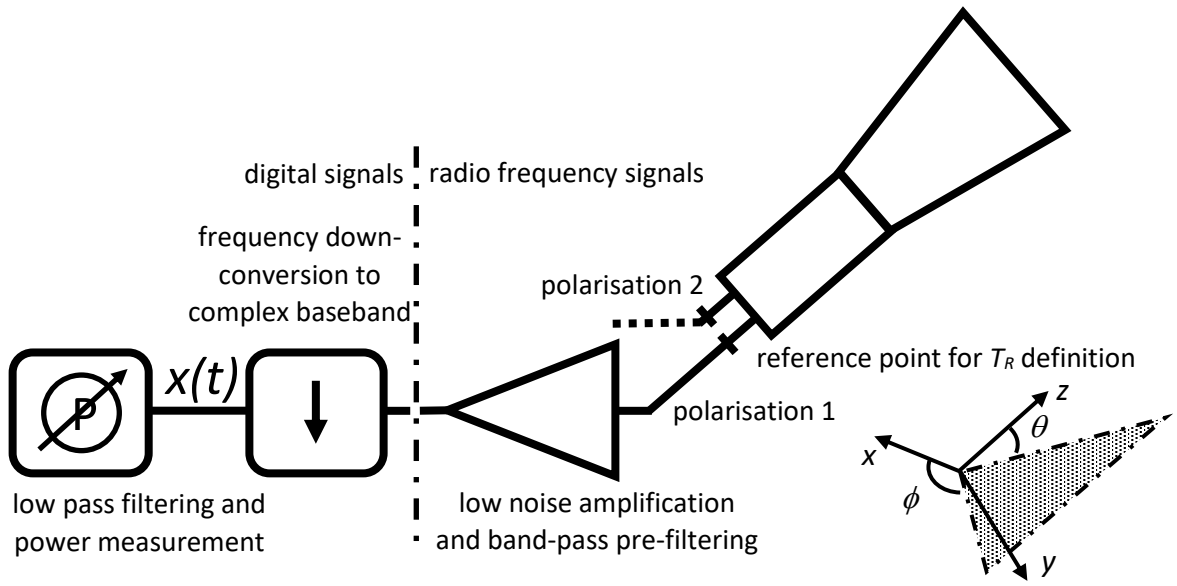

Figure 1: measurement of the cosmic microwave background radiation – idealised setup

Even though the antenna and electronics gains are real numbers in the power Eq. (2), they have to be considered, within the frame of a complex formalism used to represent narrowband signals, as the absolute modulus squared of complex numbers, with given amplitude and phase, in the case of the antenna gain dependent on both angular coordinates θ, ϕ.

$$\begin{aligned} G(\theta,\phi) &= \left|\sqrt{G(\theta,\phi)}e^{i\Phi(\theta,\phi)}\right|^2, \\ g_x &= \left|\sqrt{g_x}e^{i\varphi_x}\right|^2. \end{aligned} \tag{3}$$

The amplitude and phase components in Eq. (3) may be frequency dependent, however here we assume an ideally flat frequency response within the measured bandwidth (furthermore, for the phase we neglect any linear variation in frequency associated to a propagation delay within the system). The power on the left side of Eq. (2) therefore is due to a narrowband noise-like signal being received by the feed, which can be represented, after frequency down-conversion to complex baseband, as follows (time dependency is shown only below, and is omitted in the rest unless it is not obvious)

$$\begin{aligned} [x(t)]_{\text{point source}} &= v(t)\sqrt{g_x}e^{i\varphi_x}\sqrt{WkT_R} \\ &+ u(t)\sqrt{g_x}e^{i\varphi_x}\sqrt{\frac{1}{4\pi}WkT(\theta,\phi)\delta\Omega\sqrt{G(\theta,\phi)}}e^{i\Phi(\theta,\phi)}. \end{aligned} \tag{4}$$

In the above equation we have denoted with u and v uncorrelated realizations of complex zero-mean, stationary stochastic processes with spectrum contained in W and with unitary power

$$\begin{aligned} &E[|u|^2] = E[|v|^2] = 1, \\ &E[v^* u] = 0, \end{aligned} \tag{5}$$

with $(\cdot)^*$ denoting complex conjugation, and where $E[\cdot]$ denotes statistical ensemble expectation. In a physical scenario the radiation is received from all directions, and therefore the total received signal x is obtained by summing the components from all directions θ_i, ϕ_i

$$x = v\sqrt{g_x}e^{i\varphi_x}\sqrt{WkT_R} + \sqrt{\frac{g_x Wk}{4\pi}}e^{i\varphi_x}\sum_i u_i\sqrt{G(\theta_i,\phi_i)}e^{i\Phi(\theta_i,\phi_i)}\sqrt{T(\theta_i,\phi_i)\delta\Omega_i}, \tag{6}$$

with u_i representing the random time evolution of each component, fulfilling the same properties of u in Eq. (5). The power of the received signal x is equal to $E[|x|^2]$, and can be computed based on Eq. (6); furthermore, if the temperature field is spatially incoherent, we can assume

$$E\left[u_i^* u_j\right] = \delta_{ij}, \tag{7}$$

where δ_{ij} is equal to one if $i = j$, and zero otherwise. When using the assumption of spatial incoherency, we get, after few manipulations

$$E[|x|^2] = g_x WkT_R + \frac{g_x Wk}{4\pi}\sum_i T(\theta_i,\phi_i)G(\theta_i,\phi_i)\delta\Omega_i. \tag{8}$$

When transforming the above sum into an integral and when assuming that the spatial incoherency of the CMB temperature continues to hold in such a limit, we get the following expression

$$E[|x|^2] = g_x Wk\left(T_R + \frac{1}{4\pi}\int T(\theta,\phi)G(\theta,\phi)d\Omega\right). \tag{9}$$

Before continuing, we underline that the proportionality factor $g_x Wk$ in Eq. (9), even though important for implementation aspects, is conceptually irrelevant. We therefore assign it equal to one, assuming it has been perfectly calibrated, and redefine Eq. (9) as follows

$$T_x = T_R + \frac{1}{4\pi}\int T(\theta,\phi)G(\theta,\phi)d\Omega. \tag{10}$$

The physical quantity of interest in the above equation is of course the temperature provided by the integral component. The reason for "proving" (or rather motivating) the above well-known Eq. (10), is to emphasize the fact that it relies upon the hypothesis of spatial incoherency of the CMB radiation. The equation establishes a definite relation between a measurable quantity (T_x), a quantity whose value (possibly slowly time-varying) can be accurately calibrated (T_R), a function that can be measured "once for all" (G, the antenna radiation pattern) and the quantity of physical interest $T(\theta,\phi)$. Obviously, the effects of the angular resolution of the measurement, linked to the beamwidth of the antenna, and of the finite time integration have to be taken into account in the post-processing of the raw data. The second effect, which determines the sensitivity of the measurement process, translates unchanged into the new approach and is not addressed in this paper, whereas the aspect of angular resolution is discussed in the following section 3, when introducing the use of high order modes in a unified terminology.

3. Use of high order modes

Let us now refer to the fig. 2. The setup is equivalent to the one of fig. 1 for what concerns the power/temperature measurement, which is covered by the blocks in grey. However, an element has been added to the antenna system, to be able to couple to a high-order mode within the feed, *i.e.*, a mode with a spatial configuration which is different from the one of the dominant modes used for power detection. The amplitude of the high order mode typically decays along the direction of propagation, beyond the feed system[1]. Indeed, infinite modes are excited within the feed system by the impinging radiation, and as we will see they encode information about such radiation, which can be retrieved. Let us consider a high order mode and associated radiation pattern $H_\mu(\theta,\phi)$ (defined within the same reference frame adopted for the "main" radiation pattern G and for the CMB temperature field) once again meant to be the absolute modulus squared value of a complex number

$$H_\mu(\theta,\phi) = \left|\sqrt{H_\mu(\theta,\phi)}e^{i\psi_\mu(\theta,\phi)}\right|^2. \tag{11}$$

The index μ is equal to $1, 2, 3, \ldots$, with $\mu = 1$ representing the dominant mode (associated to the radiation pattern $G(\theta,\phi)$ defined in the previous section), and the subsequent μ identifying higher order modes.

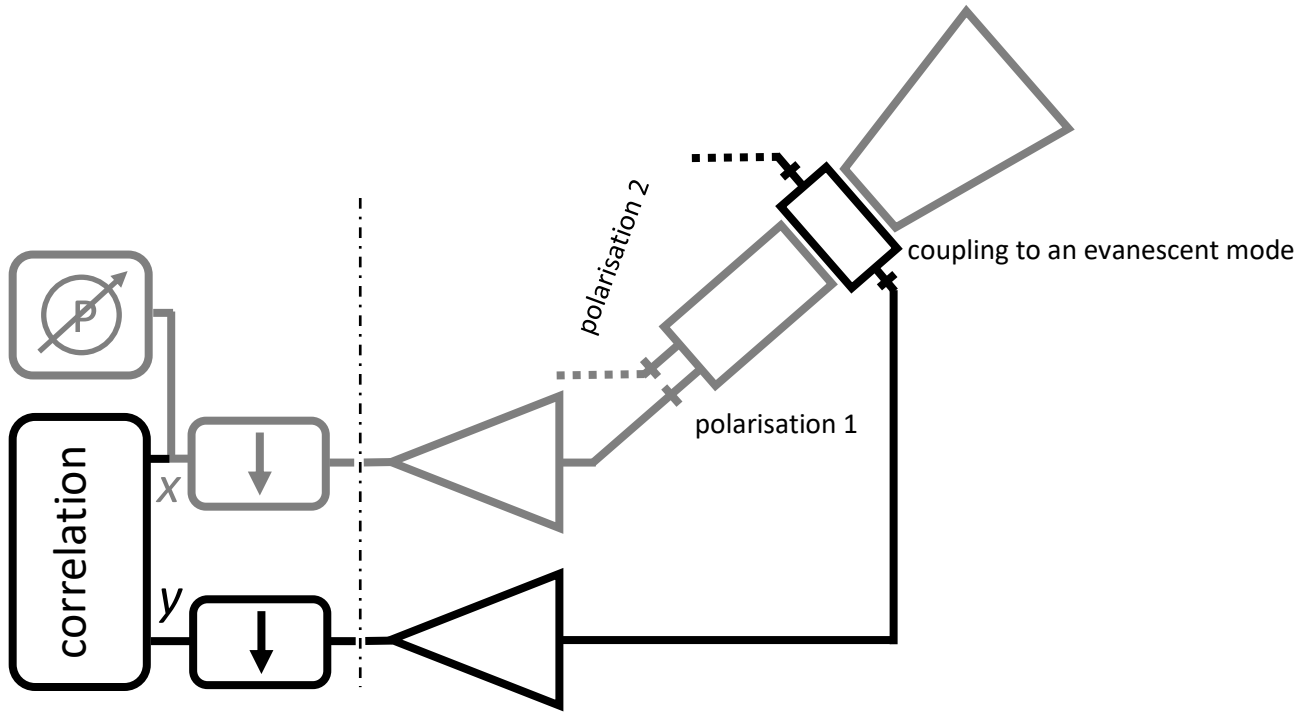

Figure 2: antenna feed system setup including coupling to an evanescent mode

By following the same steps applied in the previous section, the signal x observed through the main radiation pattern $H_1 = G$ can be expressed as in Eq. (6), and its power can be measured as previously discussed. The above means that the proposed setup preserves the functionality of that shown in fig. 1

[1] We are not considering here multi-mode feeds like those described *e.g.* in [10] and [11], in which several modes propagate and are collectively (and incoherently) detected with the main purpose of shaping the antenna power radiation pattern.

(the presence of the coupling device may imply an additional loss on the main path, which however can be made small in practical implementations). In addition to the signal x however, a signal y is also available, received through the pattern H_μ, which, following the same reasoning leading to Eq. (6), can be expressed as follows

$$y(t) = z(t)\sqrt{g_y}e^{i\varphi_y}\sqrt{WkT_{R,y}} + \sqrt{\frac{g_y Wk}{4\pi}}e^{i\varphi_y}\sum_i u_i(t)\sqrt{H_\mu(\theta_i,\phi_i)}e^{i\psi_\mu(\theta_i,\phi_i)}\sqrt{T(\theta_i,\phi_i)\delta\Omega_i}, \quad (12)$$

with the measurement bandwidth W being the same as on the main path. It is important to remark that each normalised time evolution u_i is the same in Eqs. (6) and (12) (of course if "i" scans through the same set of angular directions in the two equations), because the two involved electromagnetic modes differ among each other only in terms of spatial distribution of the field within the feed system. Furthermore, in the above equation the power gain of the electronics has been denoted with g_y, with an associated phase φ_y. Finally, z is the realization of a stochastic band-limited process of unitary power, uncorrelated with v and u_i (it is associated to dissipative effects in the feed components and subsequent electronics associated to the detection and amplification of the evanescent field, collectively labelled with $T_{R,y}$). The quantity of interest now, of which the correlator of fig. 2 provides an estimate, is the cross-correlation between the signals x and y, equal to $E[x^*y]$. The computation of such cross-correlation proceeds along the same lines as in the previous section for the computation of the power of x. In particular, the spatial incoherency of the CMB radiation must once again be invoked to obtain, in integral form, the following expression

$$E[x^*y] = \sqrt{g_y g_x}Wke^{i\left(\varphi_y-\varphi_x\right)}\frac{1}{4\pi}\int T(\theta,\phi)\sqrt{H_\mu(\theta,\phi)H_1(\theta,\phi)}e^{i\left(\psi_\mu(\theta,\phi)-\psi_1(\theta,\phi)\right)}d\Omega. \quad (13)$$

As done before, we ignore complications linked to the gain of the electronics for both paths of fig. 2 and assign the complex pre-factor to one, and redefine the observable as a (complex) temperature as follows

$$T_{\mu,1} = \frac{1}{4\pi}\int T(\theta,\phi)\Pi_{\mu,1}(\theta,\phi)d\Omega, \quad (14)$$

where we have defined the synthesized radiation pattern[2]

$$\Pi_{\mu,1}(\theta,\phi) = \sqrt{H_\mu(\theta,\phi)H_1(\theta,\phi)}e^{i\left(\psi_\mu(\theta,\phi)-\psi_1(\theta,\phi)\right)}, \quad (15)$$

[2] The indexing in definitions (14) and (15) seems redundant as one could have indexed the quantities with just an integer, without the mentioning to "1". However, in a more general approach which, even though perfectly legitimate, is not deepened here, one could correlate the mode μ with a mode ν which is different from the dominant one, *e.g.* leading to the observable $T_{\mu,\nu}$. Additional indexing could be added when wishing to correlate modes from orthogonal polarisations, which is also not deepened here.

which is in general complex, with the exception of $\Pi_{1,1} = H_1 = G$ which is real and positive. The above Eq. (14) is fully general and describes a set of observables including the current one represented by Eq. (10) when setting $\mu = 1$, i.e.

$$T_x = T_R + T_{1,1}. \tag{16}$$

However, Eq. (14) does not offer a hint for exploitation yet, and another step is required in order to identify a potential application. Indeed, it is opportune to expand both the temperature field and the synthesized radiation patterns in spherical harmonics[3]

$$\begin{aligned} T(\theta,\phi) &= \sum_{l=0}^{\infty}\sum_{m=-l}^{l} a'_{l,m} Y_{l,m}(\theta,\phi)\,, \\ \Pi_{\mu,1}(\theta,\phi) &= 4\pi \sum_{l=0}^{\infty}\sum_{m=-l}^{l} b_{l,m}^{\mu,1} Y_{l,m}(\theta,\phi), \end{aligned} \tag{17}$$

with the following definition and normalisation properties

$$\begin{aligned} &Y_{l,m}(\theta,\phi) = (-1)^m \left(Y_{l,-m}(\theta,\phi)\right)^* = \sqrt{\frac{2l+1}{4\pi}}\sqrt{\frac{(l-m)!}{(l+m)!}} P_l^m(cos\,\theta) e^{im\phi}, \\ &\int Y_{\bar{\lambda},\bar{\mu}}(\theta,\phi) Y_{\lambda,\mu}(\theta,\phi)^* d\Omega = \delta_{\bar{\lambda}-\lambda}\delta_{\bar{\mu}-\mu}, \end{aligned} \tag{18}$$

and where $P_l^m(\cdot)$ is the associated Legendre polynomial of degree l and order m. Concerning the synthesized radiation pattern, once this is known the coefficients of the expansion (17) can be computed according to

$$b_{l,m}^{\mu,1} = \frac{1}{4\pi}\int \Pi_{\mu,1}(\theta;h) Y_{l,m}(\theta,\phi)^* d\Omega. \tag{19}$$

With respect to CMB literature, we have designated the coefficients of the temperature expansion in Eq. (17) as $a'_{l,m}$ to indicate the fact that these coefficients are defined in the antenna reference frame, and therefore they do not coincide with the (un-primed) coefficients obtained over a standard reference frame. However, it is obvious that the above representation of the temperature field is unambiguously related to the representation in another frame. Due to the fact that the CMB temperature is a real quantity, the following property holds

$$a'_{l,-m} = (-1)^m \left(a'_{l,m}\right)^*. \tag{20}$$

When using the expansions of Eq. (17) in Eq. (14), and when using the properties (18), we immediately obtain

[3] The definition of the radiation pattern expansion is not unique. The selected definition leads to the behaviour of the *b*-coefficients shown in fig. 3.

$$T_{\mu,1} = \sum_{l=0}^{\infty} \sum_{m=-l}^{l} \left(a'_{l,m}\right)^{*} b_{l,m}^{\mu,1}. \tag{21}$$

The above equation illustrates how the measurement of high order modes can introduce constraints on linear combinations of the coefficients $a'_{l,m}$, with the weights of such combinations being represented by coefficients of the involved synthesized radiation pattern expansion. As it will be clear later (and as it is well known for the currently exploited $T_{1,1}$) such observables will be able to explore only degrees l up to a given maximum order $l_{\max}$, due to the finite aperture of the observing system, introducing a filtering action on the angular spectrum of the observed temperature field. In the following we select the radiation patterns of a sample antenna system, clarifying the above aspects and also allowing to estimate the amount of signal which can be detected from each observable.

4. Sample system

We make reference to radiation patterns obtained by use of a corrugated circular waveguide feed of internal radius b, for circular polarised radiation, addressed in [12] and [13], in the latter reference corresponding to the "uniform phase" approximation in Eq. (5) within the paper. The reason for selecting a corrugated circular waveguide feed is simply that closed formulas are available for the radiated field. Extension to corrugated conical horn is conceptually straightforward, and methods for computing the radiated field, requiring numerical integration, are reported in the same [13] and also in [14]. The reason for selecting corrugated structures (either waveguide of horn) is due to the possibility of obtaining pattern symmetry with respect to the azimuthal angle ϕ. When referring to [13], the following expressions of the radiated fields are available for the balanced modes $HE_{\mu 1}, \mu = 1,2,3 \ldots$ for a left-hand circular polarised radiation (similar expressions, not reported here, apply for right hand circular polarisation)

$$E_{\phi} = iE_{\theta} \propto (i)^{\mu} \frac{1+\cos\theta}{2} \cdot \frac{\mathrm{J}_{\mu-1}(\beta_0 b \sin\theta)}{(\beta_0 b \sin\theta)^2 - \zeta_{\mu}^2} e^{i\mu\phi}, \tag{22}$$

where ζ_{μ} is the first zero of the Bessel function of the first kind and order $\mu - 1$. Furthermore $\beta_0 = 2\pi/\lambda$ with λ being the centre wavelength of the observed narrowband spectrum. The left hand circular polarised component is built as follows

$$E_L = \frac{E_{\theta} - iE_{\phi}}{\sqrt{2}} e^{-i\phi} = \sqrt{2} E_{\theta} e^{-i\phi}. \tag{23}$$

Based on the above we can build the synthesized radiation patterns of Eq. (15)

$$\Pi_{\mu,1}(\theta,\phi) = \frac{(i)^{\mu-1}\sqrt{c_1 c_{\mu}}}{h^2} (1+\cos\theta)^2 \frac{\mathrm{J}_{\mu-1}(\beta_0 b \sin\theta)\mathrm{J}_0(\beta_0 b \sin\theta) e^{i(\mu-1)\phi}}{\left[(\beta_0 b \sin\theta)^2 - \zeta_{\mu}^2\right]\left[(\beta_0 b \sin\theta)^2 - \zeta_1^2\right]}, \tag{24}$$

where $h \cong 4.152/(\beta_0 b)$ is the half-power beamwidth of the antenna, and the constants c_i ensure proper normalisation of each individual power radiation pattern. Based on the above patterns, the coefficients b of Eq. (19) can be computed for each considered synthesized pattern. Due do the complex exponential term in Eq. (24), the non-zero coefficients for the synthesized pattern $\Pi_{\mu,1}$ are only those with azimuthal index m equal to $\mu - 1$. As a consequence, the observable $T_{\mu,1}$ of Eq. (21) will only depend upon the coefficients $a'_{l,\mu-1}$, each weighted by the beam coefficient $b_{l,\mu-1}^{\mu,1}$

$$T_{\mu,1} = \sum_{l=0}^{\infty} \left(a'_{l,\mu-1}\right)^* b^{\mu,1}_{l,\mu-1}. \tag{25}$$

The behaviour of the non-zero beam coefficients is shown in the following fig. 3.

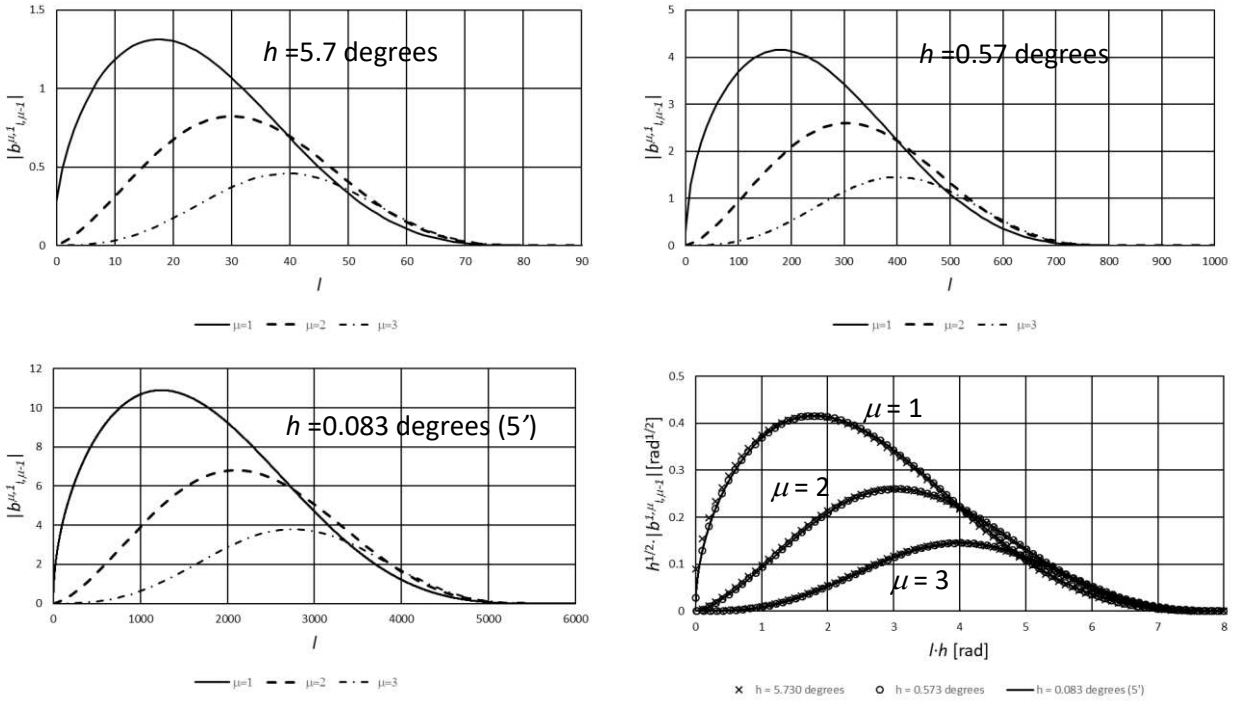

Figure 3: Behaviour of the absolute value of the beam coefficients as a function of the selected synthesized radiation pattern, of the half-power beamwidth *h* and of the angular order *l*. The figure on the bottom-right shows the coefficients properly scaled in order to collapse the curves into one for each synthesized pattern. The phase of the complex coefficients is 0, π/2 and π rad for μ = 1,2,3.

We can use Eq. (25) to get an idea of the magnitude (say δT) that can be expected from the various observables. Indeed, by assuming statistical independence of the coefficients of the CMB expansion of Eq. (17), we obtain

$$\left(\delta T_{\mu,1}\right)^2 \triangleq E\left[\left|T_{\mu,1}\right|^2\right] = \sum_{l=2}^{\infty} E\left[\left|a'_{l,\mu-1}\right|^2\right] \left|b^{\mu,1}_{l,\mu-1}\right|^2 = \sum_{l=2}^{\infty} C_l \cdot \left|b^{\mu,1}_{l,\mu-1}\right|^2, \tag{26}$$

where

$$C_l = E\left[\left|a'_{l,\mu-1}\right|^2\right], \tag{27}$$

is the so called CMB power spectrum. The above Eq. (26) has a clear intuitive meaning: the various components of the power spectrum are simply weighted through the beam coefficients, as through a filtering action (see for example the related discussion in [16] related to the current observable). The behaviour of C_l as a function of the multipole moment *l* is omnipresent in literature, here the values from [15] have been used (converted from the value reported in the file $D_l = l(l+1)C_l/2\pi$). The result is

shown in Table I, for three different half-power beamwidths. As expected, the signal from the synthesized pattern $\Pi_{1,1}$ (the current power detection method) is larger the smaller *h*, whereas this is not the case for the other observables which, in this very coarse analysis, show a peak behaviour for *h* around 0.6 degrees. The other remark is that, even though the signal from $\Pi_{1,1}$ is dominant in all scenarios, the other two signals are of not negligible magnitude, especially the one from $\Pi_{2,1}$; indeed, for the "best" *h* of around 0.6 degrees, the signals from $\Pi_{2,1}, \Pi_{3,1}$ are a non-negligible fraction of the corresponding dominant signal.

half-power beamwidth *h* [degrees]	**δT_{11} [μK]**	**δT_{21} [μK]**	**δT_{31} [μK]**
0.083	108.0	14.0	2.5
0.573	83.1	27.8	9.3
5.730	41.4	13.4	5.4

Table I: Estimated magnitude of the temperature signal which can be expected when using the proposed observables, including the existing one (δT_{11}) as well as the newly proposed (δT_{21} and δT_{31}) as function of the half-power beamwidth. The estimates do not take into account any efficiency or implementation loss which will reduce the actual magnitudes, which is unimportant for a comparative analysis.

It is also simple to show that, in view of their definition, and when assuming statistical independence of the coefficients $a'_{l,m}$, the observables defined in Eq. (25) are orthogonal.

$$E\left[\left(T_{\mu,1}\right)^{*} T_{m,1}\right] = 0, \mu \neq m. \tag{28}$$

5. Conclusions and future work

We have introduced new observables of the CMB: they can be formed by detecting, within the antenna system of a space observatory, high order modes of the received electromagnetic field, to be coherently combined with the main mode already used for power detection. The new observables provide distinct linear combinations of the coefficients of the expansion of the CMB temperature, of a reasonable magnitude to be detected.

This work is only the first step of a roadmap which should include 1) a deeper analysis of the new observables, to link them to the existing theoretical framework in cosmology, and also to define in detail the experimental setup, e.g. including polarisation aspects, sizing of the half-power beamwidth for best response, selecting high order modes and feed structure, etc. 2) manufacturing a test feed system to verify the practical feasibility of the approach and finally 3) flying an observatory including the measurement of new observables in addition to the currently used.

All in all, we believe that, in order to balance the efforts devoted to the establishment of theoretical frameworks in cosmology, it is essential to enrich the experimental dataset, not only by increasing the performance of current observables, but also by introducing diverse and complementary ones.

6. References

[1] Penzias, A. A. and Wilson, R. W., "A Measurement of Excess Antenna Temperature at 4080 Mc/s.", The Astrophysical Journal, vol. 142, pp. 419–421, 1965. doi:10.1086/148307.

[2] Durrer, Ruth. "The cosmic microwave background: the history of its experimental investigation and its significance for cosmology." Classical and Quantum Gravity 32.12 (2015): 124007

[3] Strukov, I. A., Brukhanov, A. A., Skulachev, D. P., and Sazhin, M. V., “Anisotropy of relic radiation in the RELICT-1 experiment and parameters of grand unification”, Physics Letters B, vol. 315, no. 1–2, pp. 198–202, 1993. doi:10.1016/0370-2693(93)90180-P
[4] John C. Mather, "Cosmic background explorer (COBE) mission," Proc. SPIE 2019, Infrared Spaceborne Remote Sensing, (1 October 1993); https://doi.org/10.1117/12.157821
[5] Hinshaw, Gary, et al. "Nine-year Wilkinson Microwave Anisotropy Probe (WMAP) observations: cosmological parameter results." The Astrophysical Journal Supplement Series 208.2 (2013): 19.
[6] Ade, Peter AR, et al. "Planck 2013 results. I. Overview of products and scientific results." Astronomy & Astrophysics 571 (2014): A1.
[7] Fixsen, D. J. "The temperature of the cosmic microwave background." The Astrophysical Journal 707.2 (2009): 916.
[8] Lamarre, J-M., et al. "Planck pre-launch status: The HFI instrument, from specification to actual performance." Astronomy & Astrophysics 520 (2010): A9.
[9] Bersanelli, Marco, et al. "Planck pre-launch status: Design and description of the Low Frequency Instrument." Astronomy & Astrophysics 520 (2010): A4.
[10] Murphy, J.Anthony and R. Stewart Padman. “Radiation patterns of few-moded horns and condensing lightpipes.” Infrared Physics 31 (1991): 291-299.
[11] Padman, R. Stewart and J.Anthony Murphy. “Radiation patterns of “scalar” lightpipes.” Infrared Physics 31 (1991): 441-446.
[12] L. Sakr, "The higher order modes in the feeds of the satellite monopulse tracking antennas," 11th IEEE Mediterranean Electrotechnical Conference (IEEE Cat. No.02CH37379), 2002, pp. 453-457, doi: 10.1109/MELECON.2002.1014634
[13] A. Densmore, Y. Rahmat-Samii and G. Seck, "Corrugated-Conical Horn Analysis Using Aperture Field With Quadratic Phase," in IEEE Transactions on Antennas and Propagation, vol. 59, no. 9, pp. 3453-3457, Sept. 2011, doi: 10.1109/TAP.2011.2161552.
[14] Clarricoats, P. J. B., and P. K. Saha. "Propagation and radiation behaviour of corrugated feeds. Part 2: Corrugated-conical-horn feed." Proceedings of the Institution of Electrical Engineers. Vol. 118. No. 9. IET Digital Library, 1971.
[15] European Space Agency, “A dataset provided by the European Space Agency File”, file “COM_PowerSpect_CMB-TT-full_R3.01”, https://doi.org/10.5270/esa-gb3sw1a
[16] Aghanim, N., et al. "Planck 2013 results. IV. Low Frequency Instrument beams and window functions." Astronomy & Astrophysics 571 (2014): A4.

Author’s contribution
ML and RD jointly prepared, reviewed and approved the manuscript.

Ethics Declaration
Conflict of interest: The authors declare that there are not conflicts of interest.

Availability of Data and Materials
The corresponding author can be contacted for provision of data and materials used for the preparation of the manuscript.

Acknowledgements
Not applicable

Funding
No funding was obtained for this study.